Nonlinear Hydrodynamic Force Relevance for Heaving Point Absorbers and Oscillating Surge Converters.

Giuseppe Giorgi*, Markel Penalba†, John V. Ringwood‡
Centre for Ocean Energy Research
Maynooth University
Maynooth, Co. Kildare, Ireland
Email: *ggiorgi@eeng.nuim.ie, †mpenalba@eeng.nuim.ie, ‡john.ringwood@eeng.nuim.ie

***Abstract*—Two of the most common modes of oscillation of single degree of freedom wave energy converters are heave and surge, which are respectively exploited by heaving point absorbers (HPAs) and oscillating surge converters (OSCs). Notwithstanding essential hydrodynamic differences, both devices are very often described by the same linear model structure. However, if the linearising assumption of small amplitudes of motion is challenged, especially under controlled conditions, different (and significant) nonlinearities are excited in the devices.**

This paper studies the differences between the hydrodynamic forces in HPAs and OSCs under controlled conditions, considering a nonlinear representation of Froude-Krylov forces and viscous drag effects. Results show that HPAs are predominantly affected by nonlinear Froude-Krylov forces, while the most important hydrodynamic forces in OSCs are due to diffraction and radiation effects. In addition, viscous drag appears to have little relevance in HPAs but a significant influence in OSCs.

***Index Terms*—Wave energy, nonlinear Froude-Krylov force, viscous drag, heaving point absorbers, oscillating surge converters.**

I. Introduction

Wave energy converters (WECs) are very often classified based on the operating principles they use to absorb energy from ocean waves. In wave activated WECs, such operating principles refer to the modes in which the device oscillates due to the action of the waves. Two of the most common modes are heave and surge, which are exploited respectively by heaving point absorbers (HPAs) and oscillating surge converters (OSCs). Notwithstanding major hydrodynamic differences [1], HPAs and OSCs are usually described by the same linear model structure, mainly due to computational convenience. Nevertheless, the underlying assumption of small motion is usually invalid, since the aim of any wave energy device (especially under the influence of energy-maximising control) is to exaggerate the motion amplitude in order to increase the power capture. As a consequence, when large oscillation amplitudes occur, linear models are inappropriate, providing unrealistic and misleading results.

The essential feature that discriminates between HPAs and OSCs is the total hydrodynamic force they experience, which, assuming the superposition principle being valid, can be divided into four different components: radiation, diffraction, Froude-Krylov (FK) and viscous drag forces. Major candidates to incorporate nonlinear effects into the system appear to be FK and viscous forces, while the linear formulation of diffraction and radiation forces is assumed to be accurate enough, especially when the characteristic length of the device is much smaller than the wave length [2], [3].

The impact of nonlinear FK force and viscous drag on the overall device dynamics depends on their relative relevance with respect to total hydrodynamic force and strongly depends on the device shape and operating principle; hence, significant differences are to be expected between HPAs and OSCs.

FK forces are defined as the integral of the static and dynamic pressure of the undisturbed incident wave field over the wetted surface of the device. Nonlinearities arise from variations in the instantaneous wetted surface, resulting from a non-uniform cross sectional area (CSA) in the direction of motion and from the relative difference between body displacement and free surface. Different approaches for nonlinear FK force representation for HPAs can be found in the literature [4]–[6], while, to the best knowledge of the authors, no nonlinear FK force models have been ever applied in OSCs.

Viscous drag, which is neglected in linear models, depends on the geometric characteristics of the device, such as the presence of sharp edges, and on the relative velocity between the device and the fluid particles. A common approach used to describe the drag force is a semi-empirical formulation based on the Morison equation [7], which has been applied in previous studies on HPAs [8], [9] and OSCs [9], [10].

Apart from effects due to the geometry of the device, nonlinear effects can be enhanced by the dynamics of the systems, i.e. an extended range of velocity and displacement. Therefore, the control strategy, which aims to increase the power absorption by enlarging the operational space, plays a crucial role in the excitation of nonlinearities, as shown in [11]. The aim of this paper is to study the relevance of nonlinear FK force and viscous drag in HPAs and OSCs under controlled conditions.

The reminder of the paper is organized as follows: Section II presents a detailed formulation of the nonlinear hydrodynamic models. A case study is presented in Section III and results

are given in Section IV. Some conclusions and final remarks are presented in Section V.

II. Hydrodynamic models

The devices studied in this paper are a heaving point absorber and an oscillating surge converter, as shown in Fig. 1. Both devices are constrained to move in a single degree of freedom, translating along the vertical direction z in the case of the HPA and pitching around the hinge with angle δ in the case of the OSC. More detailed illustrations of the HPA and the OSC are shown in Figures 2 and 3, respectively.

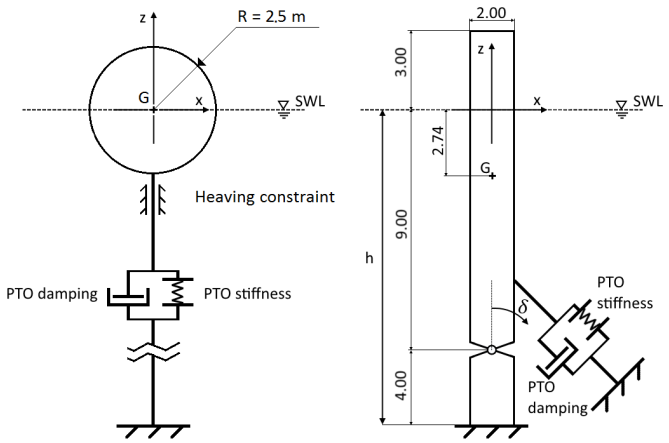

Fig. 1. Devices under study: On the left, a spherical heaving point absorber in deep water with radius R of 2.5 m with the centre of gravity G at the still water level (SWL); on the right, a prismatic oscillating surge converter, hinged at 4 m from the sea bottom and piercing the SWL at the vertical position. Both devices have a power take-off (PTO) system with a damping and a stiffness term. The PTO representation for the OSC is simply conceptual since the actual PTO operates on the rotational quantities of δ and $\dot{\delta}$.

Assuming the fluid to be inviscid and the incident flow to be irrotational and incompressible, Newton's second law of dynamics can be applied to the HPA in (1a) and to the OSC in (1b):

$$m\ddot{\mathbf{z}}(t) = \mathbf{F}_g - \iint_{S(t)} P(t)\ \mathbf{n}\ dS + \mathbf{F}_{PTO}(t) \quad (1a)$$

$$I\ddot{\boldsymbol{\delta}}(t) = \mathbf{F}_g \times \mathbf{L}_g - \iint_{S(t)} P(t)\ \mathbf{n}\times\mathbf{l}\ dS + \mathbf{T}_{PTO}(t) \quad (1b)$$

where m and I are, respectively, the mass of the HPA and the pitching inertia of the OSC, $\mathbf{F}_g$ is the gravity force, $\mathbf{L}_g$ the distance between the centre of gravity of the OSC and the hinge, S the submerged surface, P the pressure of the fluid on the body surface, $\mathbf{n}$ the vector normal to the infinitesimal surface dS, which is a distance $\mathbf{l}$ from the hinge in the case of the OSC. Finally, the power take-off system applies a force $(\mathbf{F}_{PTO})$ on the HPA and a torque $(\mathbf{T}_{PTO})$ on the OSC.

Applying Bernoulli's equation to the incident flow, the formulation of the pressure P is obtained as:

$$P(t) = -\rho g z(t) - \rho\frac{\partial\phi(t)}{\partial t} - \rho\frac{|\nabla\phi(t)|^2}{2} \quad (2)$$

where ρ is the density of the water, g the acceleration of gravity, $-\rho g z$ the hydrostatic pressure (P_{st}) and ϕ the potential flow, which, based on linear wave theory, is composed of the undisturbed incident flow potential ϕ_I, the diffraction potential ϕ_D and the radiation potential ϕ_R:

$$\phi(t) = \phi_I + \phi_D + \phi_R \quad (3)$$

Omitting the time-dependance annotation for brevity, substituting equations (2) and (3) into (1a) and (1b), and adding a viscous drag term, one obtains respectively:

$$m\ddot{\mathbf{z}} = \mathbf{F}_{FK} + \mathbf{F}_D + \mathbf{F}_R + \mathbf{F}_{vis} + \mathbf{F}_{PTO} \quad (4a)$$

$$I\ddot{\boldsymbol{\delta}} = \mathbf{T}_{FK} + \mathbf{T}_D + \mathbf{T}_R + \mathbf{F}_{vis} + \mathbf{T}_{PTO} \quad (4b)$$

where $\mathbf{F}$ and $\mathbf{T}$ are the force and torque applied on the HPA and OSC, respectively, and the subscripts FK, D, R, vis and PTO refer to FK, diffraction, radiation, viscous drag and PTO respectively. The detailed definition and implementation of each component of (4a) and (4b) is given in subsections II-A to II-D. As a common assumption, the nonlinear quadratic terms in (2) are neglected and only linear potentials are considered, since the vast majority of waves in the power production region are appropriately represented by the linear wave theory.

A. Diffraction term

The diffraction force/torque is the integral over the wetted surface of the diffraction pressure $P_D = -\rho\frac{\partial\phi_D}{\partial t}$. Assuming only small amplitude and steepness of the wave, the potential problem is linearized and solved around the equilibrium position. Therefore, the mean wetted surface S_M is considered and the diffraction term is computed through the convolution product between the diffraction impulse response function (IRF) K_D and the free-surface elevation η:

$$\mathbf{F}_R = -\iint_{S_M} P_D\ \mathbf{n}\ dS = -\int_{-\infty}^{\infty} K_D^{HPA}(t-\tau)\ \eta(\tau)\ d\tau \quad (5a)$$

$$\mathbf{T}_D = -\iint_{S_M} P_D\ \mathbf{n}\times\mathbf{l}\ dS = -\int_{-\infty}^{\infty} K_D^{OSC}(t-\tau)\ \eta(\tau)\ d\tau \quad (5b)$$

The impulse response functions for each device are obtained from the boundary element method (BEM) software WAMIT [12].

B. Radiation term

The radiation force/torque is the integral over the wetted surface of the radiation pressure $P_R = -\rho\frac{\partial\phi_R}{\partial t}$. As in Section II-A, the radiation term is computed under linear assumptions. Using Cummins equation [13], the radiation term is computed as follows:

$$\mathbf{F}_R = -m_\infty\ddot{\mathbf{z}} - \int_{-\infty}^{\infty} K_R^{HPA}(t-\tau)\ \dot{\mathbf{z}}(\tau)\ d\tau \quad (6a)$$

$$\mathbf{T}_R = -I_\infty\ddot{\boldsymbol{\delta}} - \int_{-\infty}^{\infty} K_R^{OSC}(t-\tau)\ \dot{\boldsymbol{\delta}}(\tau)\ d\tau \quad (6b)$$

where m_∞ and I_∞ are, respectively, the added mass at infinite frequency of the HPA and the added inertia at infinite frequency of the OSC, and K_R is the radiation impulse response function.

The computationally expensive radiation convolution product is replaced by its state space representation, as shown in [14].

C. Froude-Krylov term

The FK force is divided into two parts, static and dynamic, where the static FK force is the balance between the gravity force and the integral over the wetted surface of the static pressure P_{st}, while the dynamic FK force refers to the integral over the wetted surface of the dynamic pressure, derived from the incident field potential as $P_{dy} = -\rho\frac{\partial \phi_I}{\partial t}$. The integral is nonlinearly computed over the instantaneous wetted surface of the devices, considering the instantaneous intersection between the body and the free surface elevation. Due to the different shape and mode of oscillation of HPAs and OSCs, the formulation of the nonlinear FK is analyzed separately.

1) Froude-Krylov force for heaving point absorbers: Applying Airy's wave theory in deep water conditions and assuming the origin of the frame of reference at the still water level (SWL), the total pressure is obtained as follows:

$$P(x,z,t) = P_{st} + P_{dy} = -\rho g z + \rho g a e^{\chi z}\cos(\omega t - \chi x) \quad (7)$$

where x is the direction of wave propagation, a is the wave amplitude, χ the wave number and ω the wave frequency.

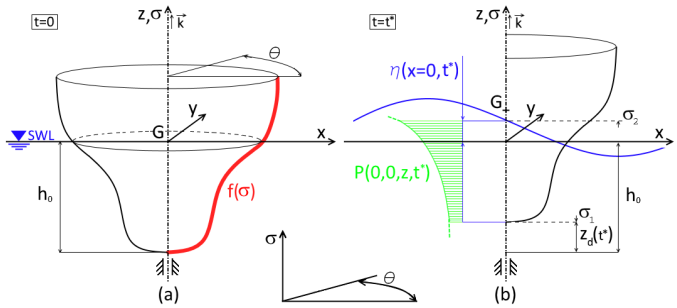

Fig. 2. Axisymmetric heaving device with generic profile $f(\sigma)$: the figure on the left shows the rest position, with the centre of gravity G at the still water level (SWL) and draft h_0; the figure on the right shows the free surface elevation η and the device displacement z_d after a time t^*. The pressure is integrated over the surface between σ_1 and σ_2 [6].

As shown in detail in [6], an algebraic solution is achievable for any axisymmetric heaving point absorber, such as the one in Fig. 2, which can be described by parametric cylindrical coordinates $[\sigma, \theta]$ as:

$$\begin{cases} x(\sigma,\theta) = f(\sigma)\cos\theta \\ y(\sigma,\theta) = f(\sigma)\sin\theta \\ z(\sigma,\theta) = \sigma \end{cases}, \quad \sigma \in [\sigma_1,\sigma_2] \wedge \theta \in [0,2\pi) \quad (8)$$

Referring to the notation in Fig. 2, the resulting FK force in heave is computed as follows:

$$F_{FK_z} = F_g - \int_0^{2\pi}\int_{\sigma_1}^{\sigma_2} P(x(\sigma,\theta),z(\sigma,\theta),t) f'(\sigma) f(\sigma) d\sigma d\theta \quad (9)$$

where the limits of integration defining the instantaneous wetted surface are $\sigma_1 = z_d - h_0$ and $\sigma_2 = \eta$.

The algebraic solution of (9) is straightforward and easily implemented in the simulation model.

2) Froude-Krylov torque for oscillating surge converters: Since the OSC is a bottom-hinged device, the pressure formulation in intermediate depth water conditions needs to be used:

$$P(x,z,t) = -\rho g z + \rho g a \frac{\cosh(\chi(z+h))}{\cosh(\chi h)}\cos(\omega t - \chi x) \quad (10)$$

where h is the water depth.

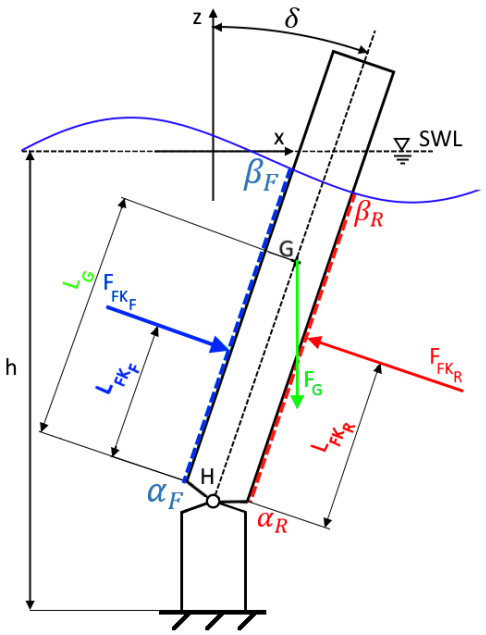

Fig. 3. Scheme for nonlinear Froude-Krylov force calculation for an oscillating surge converter. The static and dynamic pressures act on the front and rear surfaces of the flap, delimited by α at the bottom and β at the intersection between the free surface and the body.

The static and dynamic pressures simultaneously act perpendicularly on the front and rear surfaces of the OSC, which have opposite normals, generating, as a consequence, opposite torques. The torque due to the pressure on each side of the OSC is computed as the outer product between the resulting force $\mathbf{F}_{FK}$ and its distance $\mathbf{L}_{FK}$ from the hinge:

$$\mathbf{F}_{FK_F} = -\int_{-\frac{W}{2}}^{\frac{W}{2}}\int_{\alpha_F}^{\beta_F} P\,\mathbf{n}\,\frac{dx\,dy}{\sin\delta} \quad (11a)$$

$$\mathbf{L}_{FK_F} = \frac{1}{\mathbf{F}_{FK_F}}\int_{-\frac{W}{2}}^{\frac{W}{2}}\int_{\alpha_F}^{\beta_F} P\,\mathbf{n}\times\mathbf{l}\,\frac{dx\,dy}{\sin\delta} \quad (11b)$$

$$\mathbf{F}_{FK_R} = -\int_{-\frac{W}{2}}^{\frac{W}{2}} \int_{\alpha_R}^{\beta_R} P\ \mathbf{n}\ \frac{dx\ dy}{\sin\delta} \tag{11c}$$

$$\mathbf{L}_{FK_R} = \frac{1}{\mathbf{F}_{FK_R}} \int_{-\frac{W}{2}}^{\frac{W}{2}} \int_{\alpha_R}^{\beta_R} P\ \mathbf{n} \times \mathbf{l}\ \frac{dx\ dy}{\sin\delta} \tag{11d}$$

where F and R subscripts refer to the front and rear surface, respectively, and the infinitesimal area of the flap rotated by an angle δ is $dS = \frac{dx\ dy}{\sin\delta}$. The limits of integration are defined by W, which is the width of the flap along the y axis and by α and β, which define the surface on which the pressure is acting, as shown in Fig. 3. If the body is piercing the water, β is the intersection between the flap and the instantaneous free surface elevation; if the device becomes fully submerged (when large motions occur), β it is the extremity of the flap.

The total FK torque is the sum of the torque due to gravity and the torques due to the static and dynamic pressures on the front and rear surfaces:

$$\mathbf{T}_{FK} = \mathbf{F}_g \times \mathbf{L}_g + \mathbf{F}_{FK_F} \times \mathbf{L}_{FK_F} + \mathbf{F}_{FK_R} \times \mathbf{L}_{FK_R} \tag{12}$$

D. Viscous drag term

1) Viscous drag force for heaving point absorbers: The viscous drag force calculation is based on the Morison equation [7], which takes into account the shape of the device with the drag coefficient C_d, the size of the floater with the characteristic area A_d and the relative velocity between the velocity of the floater $\mathbf{V}$ and the vertical component $\mathbf{V}_{0_z}$ of the undisturbed flow velocity [9]:

$$\mathbf{F}_{vis} = -\frac{1}{2}\rho\ C_d A_d\ |\mathbf{V} - \mathbf{V}_{0_z}|\ (\mathbf{V} - \mathbf{V}_{0_z}) \tag{13}$$

Note that the characteristic surface A_d is the projection of the instantaneous wetted surface onto the plane normal to the flow. Therefore, as the the instantaneous wetted surface is considered, A_d changes as the device pierces the water during its motion.

The value of the drag coefficient C_d can be estimated for simple geometries by using the Keulegan-Carpenter number (KC), which is a dimensionless quantity defined as the ratio between drag and inertia forces acting on a body in an oscillatory fluid flow [15]. In case of sinusoidal motion, the KC number can be computed as:

$$KC = 2\pi\frac{A}{L_c} \tag{14}$$

where A is the amplitude of motion and L_c is the characteristic length scale, which is equal to the diameter, in the case of a sphere. The motion of the HPA and the diameter of the floater are of the same order of magnitude, which means that KC is about 2π, so, according to [16], C_d can be taken equal to 1. However, it is worth to point out that such method of estimating the drag coefficient is subject to some uncertainties, which could be assessed through a sensitivity analysis as shown in [9].

2) Viscous drag torque for oscillating surge converters: As in Section II-D1, the drag torque is computed by applying the Morison equation. However, since the device is rotating, the relative linear velocity between the body and the fluid is progressively changing while moving away from the hinge. Furthermore, as intermediate depth water conditions are used, the fluid velocity is significantly changing with depth due to the close presence of the bottom. Therefore, the wetted surface of the flap is equally divided into $N_s = 10$ horizontal sections and the total viscous torque $\mathbf{T}_{vis}$ is computed as follows [9]:

$$\mathbf{T}_{vis} = \sum_{i=1}^{N_s=10} \mathbf{L}_i \times \left(-\frac{1}{2}\rho\ C_d A_{d_i}\ |\mathbf{V}_i - \mathbf{V}_{0_i}|\ (\mathbf{V}_i - \mathbf{V}_{0_i})\right) \tag{15}$$

where $\mathbf{L}_i$ is the distance from the centre of the i^{th} slice to the hinge and $\mathbf{V}_i = L_i\dot{\boldsymbol{\delta}}$ is its velocity. In Section II-D1, the instantaneous wetted surface is similarly taken into account.

The number of sections N_s has been chosen equal to ten in order to have a reasonable balance between computational time and accuracy: on the one hand, the higher the number of divisions, the smaller the width of each section, the smaller the variation of the velocities with respect to the centre of the section, the higher the accuracy of the computation. On the other hand, the computational time is directly proportional to the number of sections.

The amplitude of motion of the top of the flap is likely to be of the same order of magnitude of the wave amplitude, which results in a Keulegan-Carpenter number less than one. According to [17], the drag coefficient for a plate in oscillatory flow at low KC is $C_d = 7.8KC^{-\frac{1}{3}}$, so C_d has been taken equal to 8. As already mentioned in Section II-D1, the estimation of the value of C_d is subject to some uncertainties [9].

III. Case study

Fig. 1 shows the geometries and dimensions of the HPA and the OSC which have been inspired respectively by the Wavestar HPA [18] and the Oyster 2 OSC [19].

The HPA is a sphere of radius R 2.5 m with the geometric and gravity centre at the SWL, designed to work in deep water conditions, constrained to heave (z) and tethered to the seabed through a PTO mechanism composed of stiffness and damping terms.

The OSC is a rectangular prism with dimensions of the section shown in Fig. 1 and width W equal to 26 m. The position of the centre of gravity G (2.74 m below the SWL), the mass (150000 kg) and the inertia around the hinge ($8.12{\cdot}10^6$ kgm^2), as well as all the dimensions, have been taken from [9]. The flap rotates around the hinge with angle δ and a PTO with rotational stiffness and damping terms is implemented. Note that the PTO representation in Fig. 1 is simply conceptual, since the actual PTO operates on the rotational quantities δ and $\dot{\delta}$.

Incident regular waves are used in order to study the hydrodynamic forces at each single frequency. Wave periods

T_w range from 5 s to 15 s with a 1 s step, while wave heights H_w range from 0.5 m to 3 m with a 0.5 m step.

The response of the device is analyzed under control conditions since the action of the controller enlarges the amplitude of motion and increases the relevance of nonlinearities. In order to establish an even plain field of comparison, the controller has been chosen to be the same for both the HPA and the OSC. Therefore, reactive control is applied, which tunes the stiffness and damping parameters of the PTO in order to maximize the power absorption for each sea state. Simulations show that reactive control is effective for both the HPA and the OSC as it strikes the objective of increasing the power absorption with respect to the case where the PTO acts as a linear damper (uncontrolled condition).

IV. Results

The controller, the purpose of which is to increase power absorption, has the effect of enlarging the amplitude of motion and, consequently, the relevance of nonlinearities. A comparison of the position-velocity operational space obtained in controlled and uncontrolled conditions is shown in Fig. 4, where uncontrolled conditions refer to a PTO acting as a simple proportional damper while reactive control includes both a damper and a spring term.

Fig. 4 shows a representative example of the operational spaces obtained using a regular wave of T_w 10 s and H_w 1 m for the HPA (Fig. 4(a)) and OSC (Fig. 4(b)).

Fig. 4(a) shows a dramatic effect of the controller on the operational space of the HPA. Since the wave height H_w is 1 m, the device is effectively behaving like a wave follower under uncontrolled conditions; therefore, nonlinearities are not significantly excited. On the other hand, when control is applied, the operational space gets larger and nonlinearities are likely to be important. Furthermore, nonlinearities cause a distortion of the operational space ellipse.

In the case of the OSC in Fig. 4(b), the operational space enlargement is significant but less exaggerated than in the HPA, suggesting that nonlinearities may have similar significance in uncontrolled and controlled situations.

The main differences between the HPA and the OSC arises from the relevance of each of the hydrodynamic forces in each of the devices. Figures 5(a) and 5(a) show the magnitude of the static FK (FK_{st}), dynamic FK (FK_{dy}), diffraction (D), radiation (R) and viscous drag (vis) forces and torques under controlled conditions for the HPA and the OSC, respectively, using a regular wave of $T_w = 10$ s and $H_w = 1$ m.

The nonlinear static FK term, which is the restoring force that pulls the device back into the equilibrium position, is by far the largest component in HPAs. While the dynamics of the HPAs are dominated by static and dynamic FK forces, in the OSC the major hydrodynamic action is due to diffraction and radiation forces.

The components related to wave excitation are the dynamic FK force and the diffraction force. Fig. 5 shows that HPAs are mainly excited by the dynamic FK force while, in OSCs,

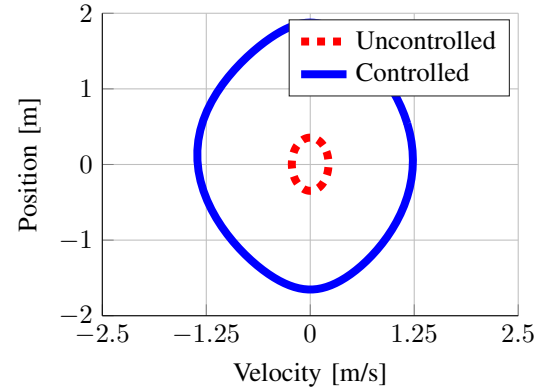

(a) Heaving point absorber.

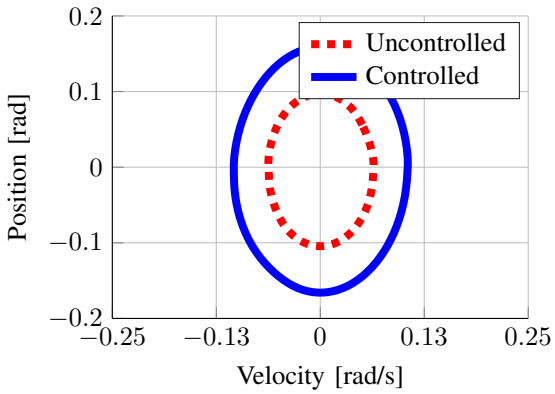

(b) Oscillating surge converter.

Fig. 4. Position-velocity operational space under uncontrolled and controlled conditions, using a regular wave of period $T_w = 10$ s and height $H_w = 1$ m.

diffraction forces are the most important wave excitation mechanism.

Radiation damping and viscous drag are the dissipative terms of the hydrodynamic force, with a notional linear and quadratic dependance on the velocity of the device, respectively. While in HPAs, dissipation terms are very small compared to the FK components, in OSCs radiation and viscous drag are predominant.

However, since the proportions of the hydrodynamic components shown in Fig. 5 depend on the input wave, the displacement and the velocity of the device, the whole range of wave periods and heights shown in Section III needs to be considered.

Fig. 6 and 7 show Froude-Krylov and drag forces normalized by the wave amplitude. Since the models are nonlinear, the curves at different wave amplitudes are distinct. Note that if the models were fully-linear, the curves of the normalized forces would perfectly overlap.

Focusing on a compact study of the relevance of nonlinearities in HPAs and OSCs, the FK ratio is defined as the ratio between the FK forces/torques (static and dynamic) and the total hydrodynamic force/torque. Likewise, the viscous drag ratio is defined as the ratio between viscous drag and the total

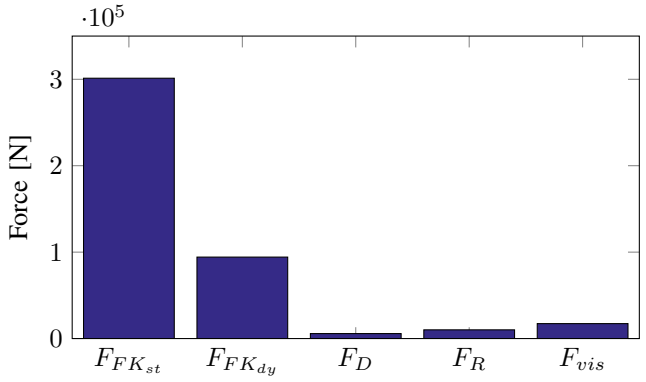

(a) Heaving point absorber.

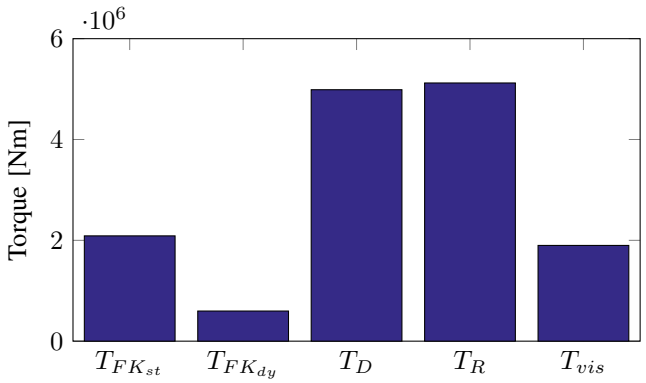

(b) Oscillating surge converter.

Fig. 5. Total hydrodynamic force (F) and torque (T) decomposition into static FK (FK_{st}), dynamic FK (FK_{dy}), diffraction (D), radiation (R) and viscous drag (vis) under controlled conditions, using a regular wave of period T_w 10 s and height H_w 1 m.

hydrodynamic force/torque.

FK and viscous drag ratios are shown, respectively, in Figures 8 and 9, where each line corresponds to a constant wave height. The HPA exhibits FK ratios from 0.81 to 0.96, showing that FK forces constitute the largest part of the total hydrodynamic force. On the other hand, FK ratios for the OSC are considerably smaller, ranging from 0.09 to 0.36. Nevertheless, both the HPA and the OSC show a similar trend: the FK ratio increases with the wave period T_w while it is independent of the wave height H_w.

The viscous drag ratio in Fig. 9 shows a completely different trend, compared to Fig. 8. The viscous drag ratio of the HPA experiences little dependence on either wave period or height, especially at larger periods, and exhibits a general slightly negative slope of the curves; since the FK forces are vastly dominating the device dynamics, as shown in Fig. 8, the variations in viscous drag force have little impact on the overall hydrodynamic force, so the viscous drag ratio remains quite small (between 0.01 and 0.06). Furthermore, the negative slope suggests that the increase in viscous drag force is even smaller than the increase in FK force. On the other hand, the viscous drag ratio for the OSC shows a strong dependance on both wave period and height. Moreover, the curves are

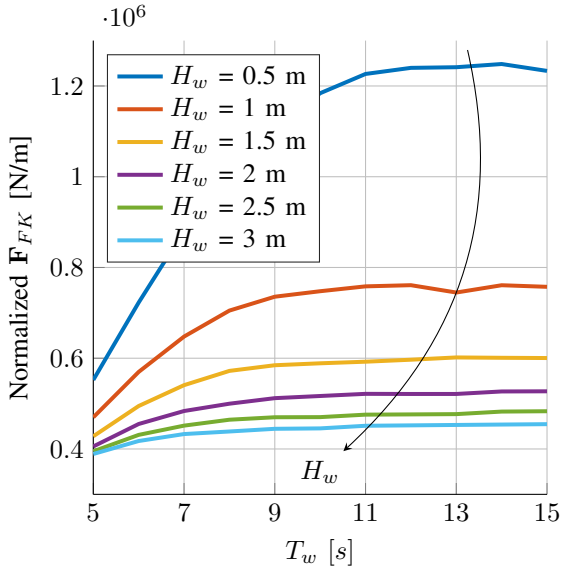

(a)

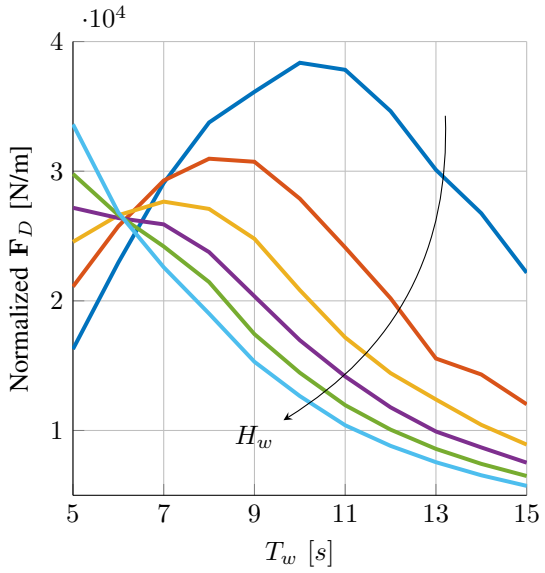

(b)

Fig. 6. Froude-Krylov $\mathbf{F}_{FK}$ and drag $\mathbf{F}_D$ force normalized by the wave amplitude $H_w/2$ for the heaving point absorber.

clearly distinct because of the large values the viscous drag ratio assumes, highlighting its relevance with respect to the total hydrodynamic force.

It is useful to gather the information contained in Figures 8 and 9 in a single compact graph, shown in Fig. 10, in order to highlight the essential differences between HPAs and OSCs and the relative importance of nonlinear FK and viscous drag effects. As shown by the arrows in Fig. 10, the cloud of points for each device presents different lines at constant wave heights H_w, increasing from left to right, with the wave period T_w increasing upwards along each line.

The cloud of points of the HPA is compact and shows little dependence on different wave height and period, occupying a

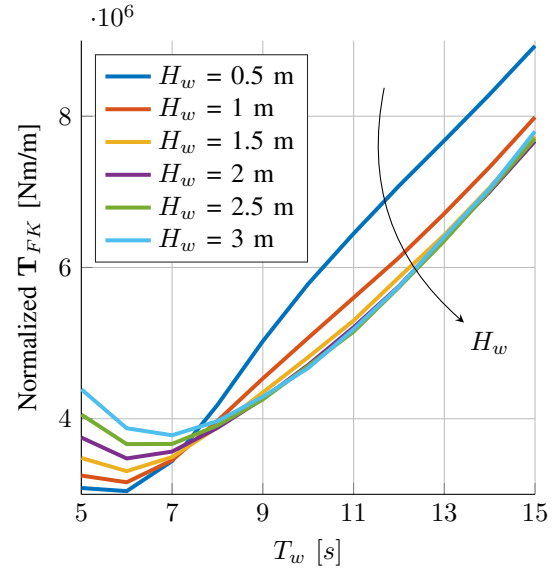

(a)

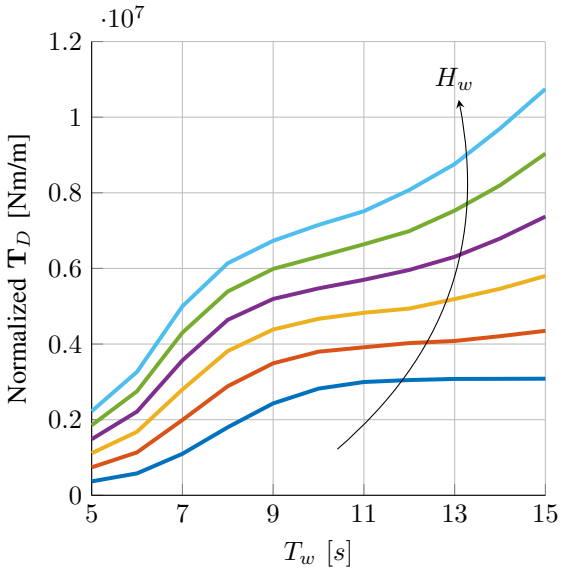

(b)

Fig. 7. Froude-Krylov $\mathbf{T}_{FK}$ and drag $\mathbf{T}_D$ torque normalized by the wave amplitude $H_w/2$ for the oscillating surge converter.

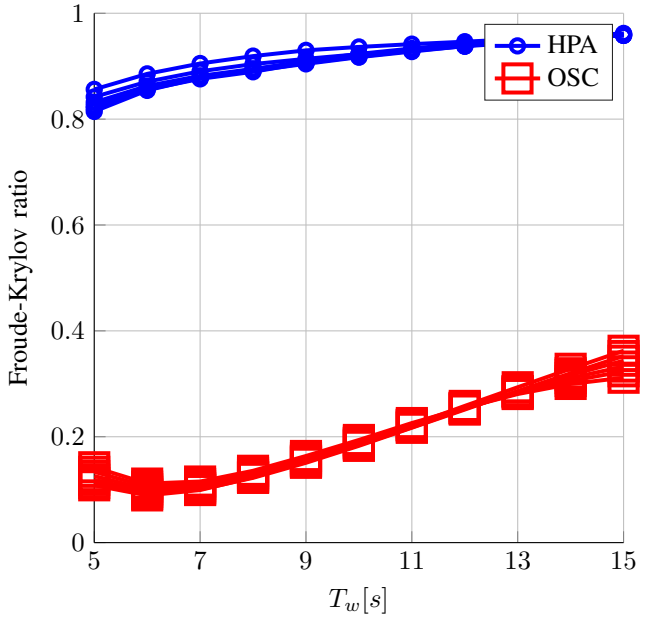

Fig. 8. Froude-Krylov force ratio, defined as the ratio between the FK force (static and dynamic) and the total hydrodynamic force. Each line has a constant wave height, ranging from 0.5 m to 3 m with a step of 0.5 m.

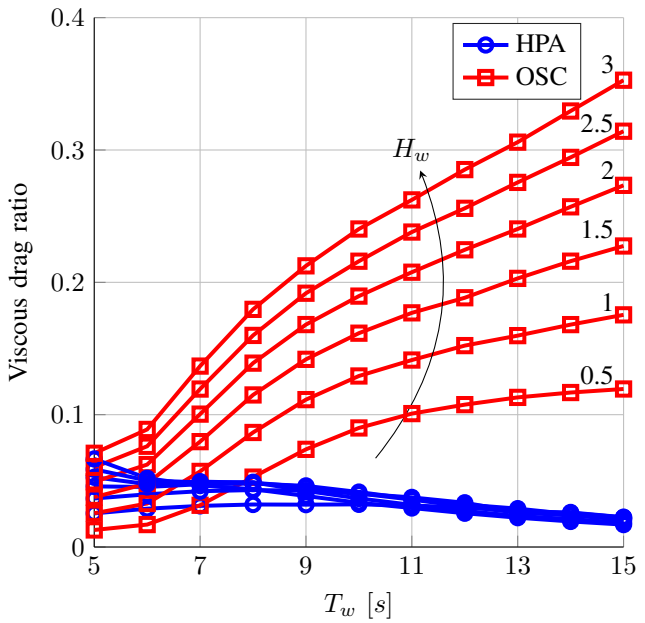

Fig. 9. Viscous drag ratio, defined as the ratio between the viscous drag force and the total hydrodynamic force. Each line has a constant wave height (shown at the right hand side), ranging from 0.5 m to 3 m with a step of 0.5 m.

small area at the top left corner of the graph at high FK ratios (greater than 0.8) and low viscous drag ratios (smaller than 0.07).

On the contrary, a completely separate region of the graph in Fig. 10 is occupied by the OSC, located at low FK ratios (lower than 0.4) and viscous drag ratios up to 0.35. The OSC cloud of points is widely spread, showing a strong sensitivity to both wave period and height.

V. Conclusion

Heaving point absorbers and oscillating surge converters are based on two very different principles of wave energy conversion, which cause them to experience very different wave-body interactions. Furthermore, under controlled conditions, the amplitude of motion increases significantly and different nonlinearities are excited in HPAs and OSCs. This paper studies the relevance of nonlinear FK force and viscous drag with respect to the total hydrodynamic force in HPAs and OSCs *under controlled conditions*.

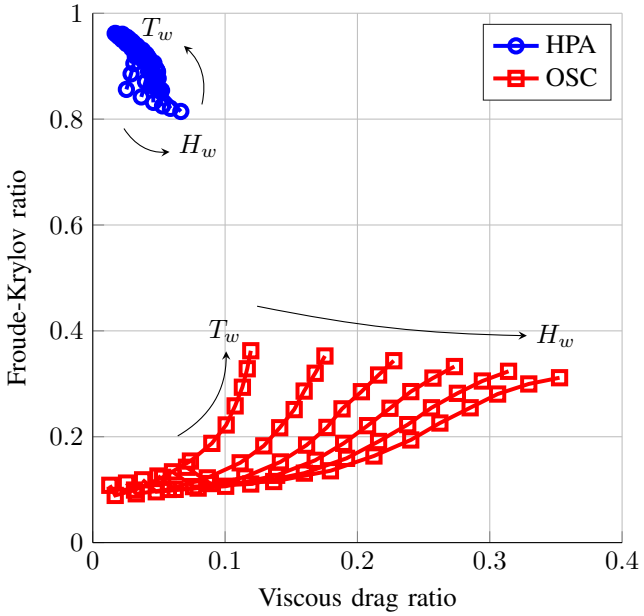

Fig. 10. Froude-Krylov ratio versus viscous drag ratio, defined as in Figures 8 and 9, respectively. Every line has a constant wave height, ranging from 0.5 m to 3 m with step 0.5 m, increasing from left to right, with wave period T_w, ranging from from 5 s to 15 s with step 1 s, increasing upwards along each line.

Viscous drag effects in HPAs are small compared to the other forces, while they are significant in OSCs. The most important hydrodynamic force in HPAs is the nonlinear FK force, while diffraction and radiation are relatively small. Moreover, the dynamic FK force is the main wave excitation mechanism in HPAs, since the diffraction force is negligible. On the contrary, the dynamics of OSCs are mainly driven by diffraction and radiation forces, while the dynamic FK force is relatively low.

Consequently, the relevance of nonlinear FK forces in HPAs appears to be considerably larger than the viscous drag, since FK forces cover 81% to 96% of the total hydrodynamic force. Such percentages remain consistent for different wave heights and periods. Conversely, the relative relevance of nonlinear FK force and viscous drag in OSCs is quite sensitive to wave parameters. Aside from the variability, FK forces are, in general, significantly more important in HPAs than in OSCs, while viscous drag becomes much more relevant in OSCs than HPAs.

Finally, it is worth to mention that a complete validation of the nonlinear models proposed in this paper is yet missing. Notwithstanding that some validation of the methods applied to describe nonlinear FK and drag forces can be found in the literature, to the best of knowledge of the authors, no previous work has used both nonlinear FK and drag force under similar controlled conditions: [5] validates nonlinear FK forces for a point absorber using the same method as in this paper, but without including viscous drag; viscous drag force using the Morison equation has been validated for a HPA [20] and OSC [21], but using a fixed body or a free decay experiment, therefore without a controller exaggerating the amplitude of motion. Finally, a first validation of the nonlinear Froude-Krylov and drag forces under control for HPA using a numerical wave tank has been proposed in [22]. The object of future work can be the complete validation of the HPA and OSC nonlinear models over a wide range of sea states and control conditions.

Diffraction and radiation forces, which have been assumed to be linear, appear to be negligible in HPAs, while they are the most important hydrodynamic force components in OSCs. As a possible topic of future work, it would be interesting to include a nonlinear representation of diffraction and radiation forces as well, which, especially in OSCs, could modify the balance between the different components of the total hydrodynamic force.

Acknowledgment

This paper is based upon work supported by Science Foundation Ireland under Grant No. 13/IA/1886.

References

[1] M. Folley, A. Henry, and T. Whittaker, "Contrasting the hydrodynamics of heaving and surging wave energy converters," *Proceedings of the 11th European Wave and Tidal Enerrgy Conference, Nantes, France*, 6-11th September 2015.

[2] J. Falnes, *Ocean Waves and Oscillating Systems*, C. UK, Ed. Cambridge University Press, 2002.

[3] A. Clement and P. Ferrant, *Nonlinear Water Waves: IUTAM Symposium, Tokyo Japan, August 25–28, 1987*. Berlin, Heidelberg: Springer Berlin Heidelberg, 1988, ch. Superharmonic Waves Generated by the Large Amplitude Heaving Motion of a Submerged Body, pp. 423–433.

[4] A. Babarit, H. Mouslim, A. Clément, and P. Laporte-Weywada, "On the numerical modelling of the non linear behaviour of a wave energy converter," in *ASME 2009 28th International Conference on Ocean, Offshore and Arctic Engineering*. American Society of Mechanical Engineers, 2009, pp. 1045–1053.

[5] J.-C. Gilloteaux, "Mouvements de grande amplitude d'un corps flottant en fluide parfait. application à la récupération de l'énergie des vagues." Ph.D. dissertation, Ecole Centrale de Nantes-ECN, 2007.

[6] G. Giorgi and J. V. Ringwood, "Computationally efficient nonlinear froude-krylov force calculations for heaving axisymmetric wave energy point absorbers," *accepted by Journal of Ocean Engineering and Marine Energy*, 2016.

[7] Morison, J.R., M., Johnson, J.W., Schaaf, and S.A., "The force exerted by surface waves on piles," *Journal of Petroleum Technology*, vol. 2, no. 5, pp. 149–154, May 1950.

[8] K. Lok, T. Stallard, P. Stansby, and N. Jenkins, "Optimisation of a clutch-rectified power take off system for a heaving wave energy device in irregular waves with experimental comparison," *International Journal of Marine Energy*, vol. 8, pp. 1–16, 2014.

[9] A. Babarit, J. Hals, M. Muliawan, A. Kurniawan, T. Moan, and J. Krokstad, "Numerical benchmarking study of a selection of wave energy converters," *Renewable Energy*, vol. 41, pp. 44–63, 2012.

[10] M. A. Bhinder, A. Babarit, L. Gentaz, and P. Ferrant, "Effect of viscous forces on the performance of a surging wave energy converter," in *Proceedings of the 22nd International and Polar Engineering Conference, Rhodes, Grece*, June 17-22 2012, pp. 545–549.

[11] M. Peñalba, A. Merigaud, J. C. Gilloteaux, and J. V. Ringwood, "Nonlinear Froude-Krylov force modelling for two heaving wave energy point absorbers," in *Proceedings of European Wave and Tidal Energy Conference, Nantes, France*, 2015.

[12] W. Inc., *WAMIT v7.0 manual*, 2013.

[13] W. Cummins, "The impulse response function and ship motion," *Schiffstechnik*, no. 9, pp. 101–109, 1962.

[14] R. Taghipour, T. Perez, and T. Moan, "Hybrid frequency-time domain models for dynamic response analysis of marine structures," *Ocean Engineering*, vol. 35, no. 7, pp. 685–705, May 2007.

[15] G. H. Keulegan and L. H. Carpenter, *Forces on cylinders and plates in an oscillating fluid*. US Department of Commerce, National Bureau of Standards, 1956.
[16] B. Molin, *Hydrodynamique des structures offshore*. Editions Technip, 2002.
[17] P. Bearman, M. Downie, J. Graham, and E. Obasaju, "Forces on cylinders in viscous oscillatory flow at low keulegan-carpenter numbers," *Journal of Fluid Mechanics*, vol. 154, pp. 337–356, 1985.
[18] "Wavestar a/s, available at http://wavestarenergy.com/."
[19] "Acquamarine power, available at http://http://www.aquamarinepower.com/."
[20] M. A. Bhinder, A. Babarit, L. Gentaz, and P. Ferrant, "Assessment of viscous damping via 3d-cfd modelling of a floating wave energy device," in *Proceedings of the 9th European Wave and Tidal Energy Conference, Southampton, UK*, 2011.
[21] ——, "Potential time domain model with viscous correction and cfd analysis of a generic surging floating wave energy converter," *International Journal of Marine Energy*, vol. 10, pp. 70 – 96, 2015.
[22] G. Giorgi, M. Penalba, and J. V. Ringwood, "Nonlinear froude-krylov force representations for heaving buoy wave energy converters," in *3rd Asian Wave and Tidal Energy Conference*, 24-28 October 2016.